INTERNATIONAL JOURNAL OF AUTOMOTIVE AND MECHANICAL ENGINEERING
ISSN: 2229-8649 e-ISSN: 2180-1606
VOLUME 22, ISSUE 2, 2025, 12483 - 12495
DOI: https://doi.org/10.15282/ijame.22.2.2025.17.0954

RESEARCH ARTICLE

Strength and Reliability of Adhesive-Bonded Joints in Semiconductor Packaging: A Computational Analysis

Shah Mohammad Azam Rishad, Md Shahidul Islam, Md Ashraful Islam*

Department of Mechanical Engineering, Khulna University of Engineering & Technology, Khulna-9203, Bangladesh

ABSTRACT – Adhesive bonded joints are increasingly used in various industries due to their enhanced structural integrity and reliability. However, successful implementation depends on understanding factors such as bond thickness. It is in fact, a crucial parameter for strength and reliability. By exploring the bond thickness and joint strength relationship, strategies can be developed to overcome vulnerabilities in the semiconductor industry, especially in chipset packaging. This study presents enhanced joint designs and their reliability. Computational analysis of adhesive-bonded joints with polymorphic bond thickness is carried out using the Finite Element Method to study the effects of bond thickness. Three-dimensional models of the adhesive-bonded connections are being developed using software with bond thicknesses ranging from 1 nm to 100 nm. Results show that at 100 nm thickness, the maximum normal stress reached approximately 3.66 MPa at the GaN-resin interface, compared to 2.55 MPa at the InN-resin interface. Shear stress peaked symmetrically around 45°, while displaying sharp drops from peak values near 0° to almost zero by 90°, depending on thickness. Stress singularity intensity decreased as adhesive thickness was reduced, indicating less stress concentration. Notably, joints with GaN exhibited 43.5% higher peak stress values compared to InN under identical conditions. This study elucidates insights regarding the intricate relation between resin thickness and joint performance, shedding light on their mechanical behavior and providing valuable data on the modal analysis for different substrates. Overall, the study reveals that varying resin thicknesses significantly affect stress distribution and vibrational behavior in adhesive-bonded joints, providing insights into joint performance and potential improvements in modern engineering.

ARTICLE HISTORY
Received : 27th July 2024
Revised : 15th Apr. 2025
Accepted : 21st May 2025
Published : 27th June 2025

KEYWORDS
Adhesive bonded joints
Numerical analysis
Nano bond thickness
Stress singularity
Chipset packaging

1. INTRODUCTION

Adhesive bonding, a vital process for creating strong material connections, has broad applications across diverse sectors. Its benefits include weight reduction, cost-effective fabrication, and damage resilience, especially in fiber-reinforced composites te. Adhesive joints offer versatility, connecting complex geometries with fatigue resistance, though challenges arise with varied thicknesses [2]. To meet the need for compact electronic devices, chipsets use adhesive-based joints that provide both structural support and stable electrical performance [3]. According to Guo et al., considering the strength and stiffness of an adhesive structure to maintain dimensional stability during vibrations and shocks, it may be necessary to design a very thin adhesive layer, possibly in the range of tens or even a few microns. Studying the mechanical behavior of highly precise adhesive joints becomes particularly difficult due to the complexities involved [4]. Investigations concentrate on the durability of bonded connections, emphasizing flat lap surfaces. Lee et al. [5] delved into the fracture resistance of bonded connections. Liao et al. [6] utilized FEA to examine mixed-mode ruptures comprehensively. Aerospace joints endure multiple loads, prompting research into epoxy polymer behavior under cyclic loading [7]. Researchers also formulated a stress transmission model, revealing an inverse relationship between stress concentration and adhesive layer thickness [8]. Chai explored fracture propagation in adhesive fixed joints, using a high-magnification video and deriving a crack energy formula [9]. Lin and Liechti investigated fatigue in diverse geometry specimens [10].

In the case of flip-chip-on-flex (FCOF) packages, researchers like Uddin et al. (2009) uncovered insights into anisotropic conductive adhesive film (ACF) utilization. ACF, comprising an epoxy matrix with minimal electrically conductive particles, poses challenges in reliable packaging techniques, necessitating ongoing advancements. Recent studies delve into criteria impacting ACF performance, with adhesion strength crucial for flip chip on flex package reliability [11]. Koguchi and Costa investigated stress singularity in 3D-bonded objects with tilted side surfaces [12]. Islam and Koguchi [13]employed BEM to scrutinize stress singularity patterns in dissimilar material connections with transversely isotropic piezoelectric attributes. Islam et al. also probed the eigen analysis method to determine stress concentrations near the free edge, suggesting a potential interface delamination risk [14]. These researchers often simplify calculations by using I-shaped or L-shaped models as smaller, generalized representations of larger configurations, although they are not at the nano level and not specifically about chipset packaging.

***CORRESPONDING AUTHOR | Md. Ashraful Islam** | ✉ md.islam@me.kuet.ac.bd

Lan et al. [15] explored the influence of epoxy resin thickness on the intensity of stress at joint interfaces, using approaches focused on stress singularities. In a related effort, Zhang et al. [16] developed mesh-independent strategies to accurately assess stress concentrations in bonded adhesive joints. However, while these studies have significantly advanced the understanding of fracture behavior and stress singularities in adhesive joints, several critical limitations remain. Most prior investigations focused on stress intensity using idealized configurations and traditional methods, often omitting analysis at the nano-scale or overlooking material systems specifically relevant to semiconductor packaging. For example, studies such as those by Kundurthi et al. [17], Korbel et al. [18], Sawa et al. [19], and Noda et al. [20] concentrated on optimizing joint parameters, but their analyses were confined to macro-scale assemblies and lacked consideration of the intricate geometries commonly encountered in sophisticated devices like microelectronics. Recent research has shown that modifying the nano-scale architecture of structural adhesives used in aerospace can greatly improve the strength and durability of bonded joints, increasing their suitability for demanding aerospace and aviation environments [21]. Kim et al. conducted numerical analyses on the capabilities of 3D piezoelectric devices connected to various structures [22]. Adhesive-bonded joints are critical in semiconductor packaging due to the presence of dissimilar materials and nano-structures. Stress singularities at material junctions have been shown to strongly correlate with interfacial failures, making them key indicators of structural reliability [23-26].

Fracture behavior, especially in EMC–Si interfaces, further complicates performance, as cohesive strength and stiffness vary significantly[26]. Additionally, accurate reliability assessment in flip-chip packages requires accounting for both singular and non-singular stress components near bonded corners[27]. These challenges underscore the necessity of precise stress modeling in adhesive-bonded joints to ensure chipset packaging integrity. So, substantial studies have scrutinized the stress field in adhesive bonded connections. Many current studies on adhesive joints concentrate on intricate, large-scale geometries, frequently neglecting the examination of smaller or scaled-down forms, such as micro- or nano-scale models, that could effectively capture diverse and irregular design variations. The uniform I-shaped nano-structure acts as a common and generalized fragment for various trimaterial bonded joints. In cases where the lower adherend is larger than the upper one, the resulting nano-structure takes on an L-shaped form.

A nano-scale L-shaped configuration is employed in this research to illustrate just one among numerous possible design variations. This particular geometry is deliberately selected because it intensifies stress at the adhesive layer's corner interface—something a straight I-shaped model does not achieve. By concentrating stress in this critical vertex zone, the model allows for more detailed observation of material responses. The interaction between design parameters and the corresponding stress patterns within adhesive joints is notably complex and difficult to predict. Variations in both material composition and structural design lead to diverse stress outcomes and distinct mechanical responses. However, the study on stress dispersion and stress magnitude factor of adhesive bonded joints with different bond thicknesses is limited. The nano-level calculation makes the stress dispersion at the apex and interface edge of three-dimensional adhesive-bonded connections quite challenging. Therefore, in the case of this study, the stress dispersion and stress intensity factor at the vertex and interfacial edge are being scrutinized in 3D adhesive-bonded connections.

2. METHODS AND MATERIAL

2.1 Geometry of the model

This study delves into two distinct tri-material joints featuring – GaN (Gallium Nitride) - SiC (Silicon Carbide), and InN (Indium Nitride) - SiC (Silicon Carbide). These joints resist moisture-induced chip damage by employing a resin middle layer for both abovementioned joints. They are recognized for their unparalleled chip-packing prowess, particularly minimal post-hardening shrinkage and hydrophobic attributes. Certain polymers within the resin contribute robust thermal conductivity, mitigating heat-related challenges and potential failures. For numerical simulation, CAD models illustrate the entire body and one-fourth, as is shown in Figure 1(a) and 1(b).

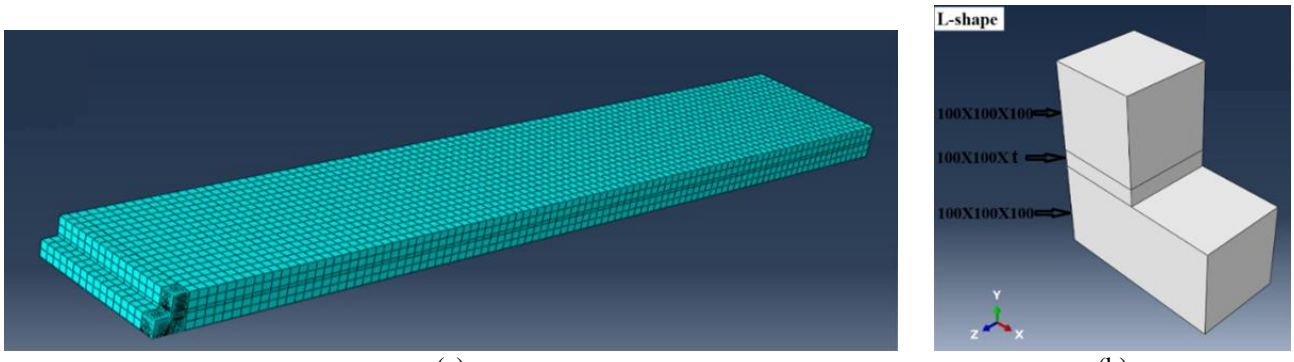

(a) (b)

Figure 1. CAD model of (a) full body and (b) one-fourth of the body

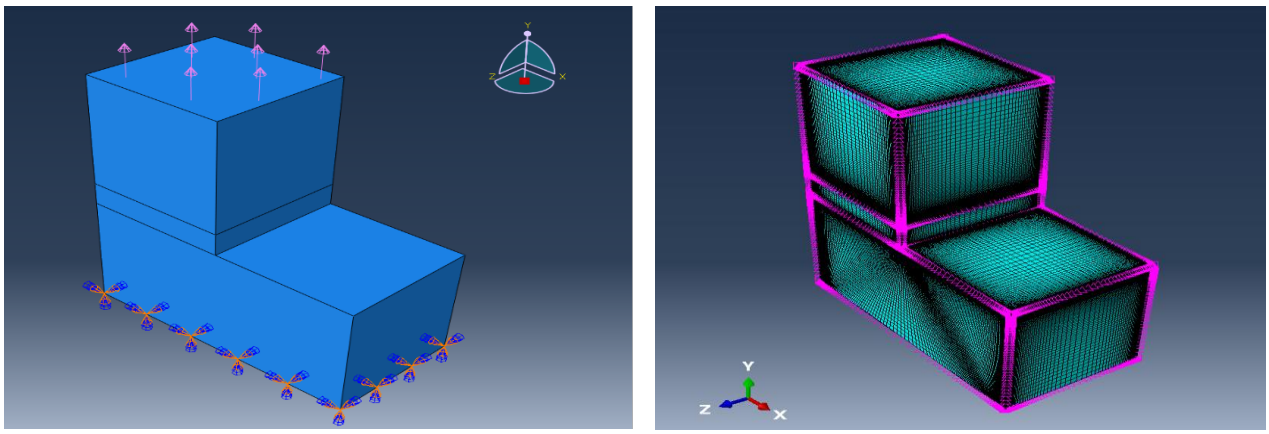

Figure 2. Analysis model with applied load and mesh generation (seeding)

The working model with load is provided in Figure 2. Here, the model is clamped under the lower adherend, and at the upper adherend, 1MPa tensile force is applied. Many forces are applied to the bonded joints. Figure 3 illustrates the trajectory of the coordinate system, specifically highlighting the radial distance (r), circumferential angle (ϕ), and radial angle (θ).

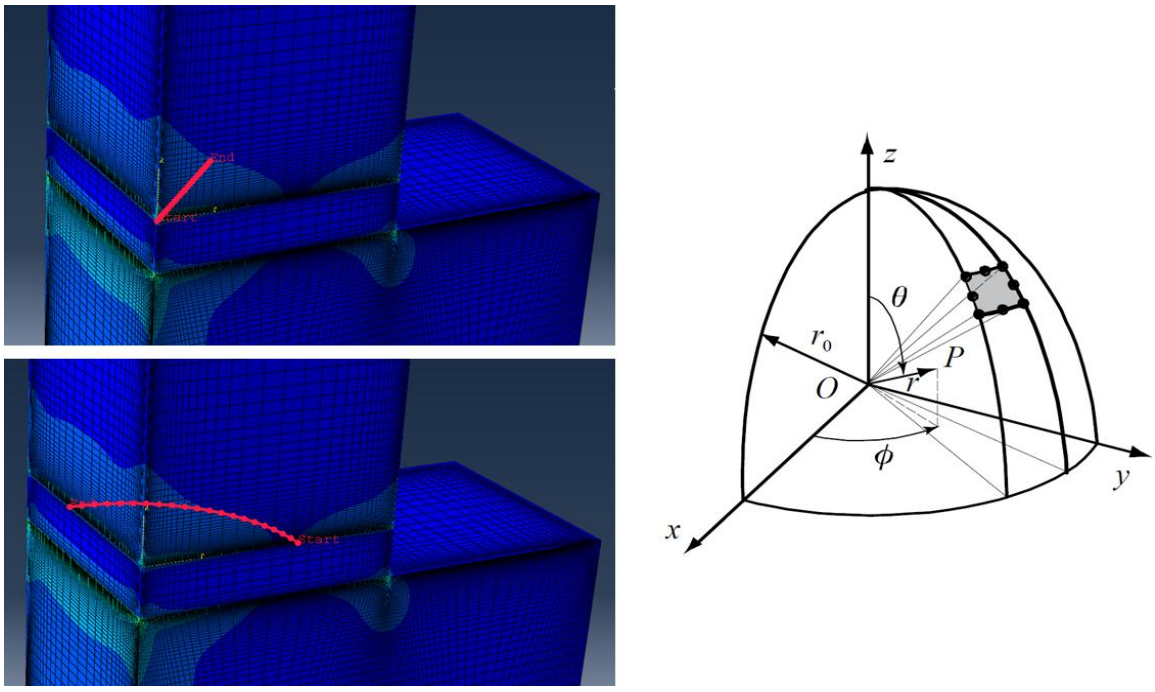

Figure 3. Path of the coordinate system (r, ϕ, θ)

Figures 2 and 4 illustrate the mesh seeding and meshing configurations applied at critical regions. The displayed mesh was generated using Abaqus, where element-based biased seeding was implemented along both vertices and edges. Specifically, horizontal edges were assigned a double bias, while vertical edges were meshed with a single bias. This approach allowed for a finer mesh concentration at the most critical joint area—where stress accumulation is expected. In this study, the C3D8E element type, an 8-node brick element, is applied to generate the mesh. The biasing method of meshing by number achieves finer mesh near the vertex region.

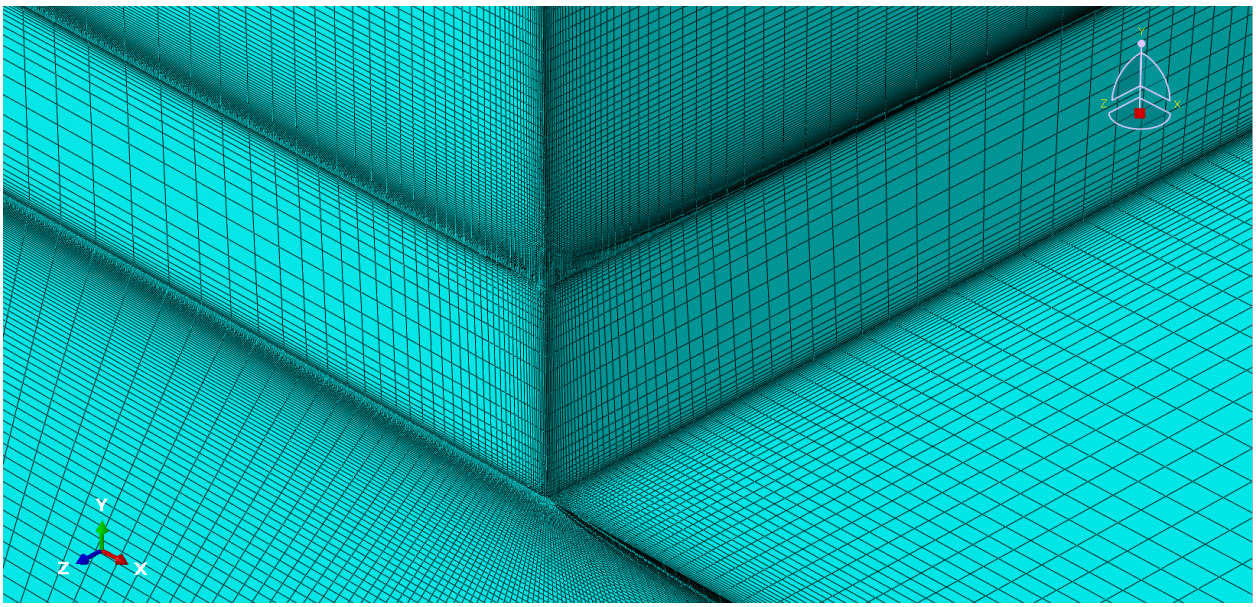

Figure 4. Mesh Distribution at the Critical Interface Region (Upper Adherend–Adhesive–Lower Adherend)

2.2 Material properties

The mechanical properties of the utilized materials for this analysis are given in Tables 1 and 2. Also, the densities of the joint materials are provided in Table 3.

Table 1. Attributes of the gallium nitride model

Material	Position	Young's Modulus (N/nm^2)	Poisson Ratio
Gallium Nitride (wurtzite)	Upper Adherend	227 e-09 [28]	0.183 [28]
Epoxy Resin	Adhesive	2.92 e-09 [28]	0.38 [28]
Silicon Carbide	Lower Adherend	166 e-09 [28]	0.26 [28]
Gallium Nitride (wurtzite)	Upper Adherend	227 e-09 [28]	0.183 [28]

Table 2. Attributes of the Indium Nitride model

Material	Position	Young's Modulus (N/nm^2)	Poisson Ratio
Indium Nitride (wurtzite)	Upper Adherend	184 e-09 [29]	0.17[29]
Epoxy Resin	Adhesive	2.92 e-09 [28]	0.38[28]
Silicon Carbide	Lower Adherend	166 e-09 [28]	0.26[28]
Indium Nitride (wurtzite)	Upper Adherend	184 e-09 [29]	0.17[29]

Table 3. The joint's density of material properties

Material	Density (kg/nm^3)
Gallium Nitride (GaN)	6.15 e-24 [30]
Indium Nitride (InN)	6.81 e-24 [31]
Epoxy Resin	1.1 e-24 [32]
Silicon Carbide (SiC)	3.21 e-24 [33]

2.2 Analysis Validation

To confirm the accuracy of the analysis, the setup was matched with the conditions outlined in reference [23], as detailed in Table 4. A 2 mm adhesive layer was used to maintain consistency in material properties and geometric dimensions for reliable comparison. Once the analysis had been validated, subsequent adjustments to materials and dimensions (nano) were made to explore a broader spectrum of scenarios and gain comprehensive insights into the tensor stress curvatures later. The maximum error was achieved at 1.085520823% compared to the reference paper. The tensor distribution of stress $\sigma_{\theta\theta}$ was plotted against the dimensionless distance parameter. The plot was then compared with the

reference paper plot [28]. The error for each work was then calculated, and the minimum error was 0.008436344%, where the paper plot was 2.28216 MPa, and the present plot was 2.282352531 MPa against dimensionless distance 0.01521.

Table 4. Comparison of the analysis to reference [23]

Dimensionless Distance r/t	Paper Stress (MPa)	Present Stress (MPa)	Error (%)
0.00824	2.94809	2.953864303	0.195865892
0.01019	2.67667	2.675466605	0.044958669
0.01521	2.28216	2.282352531	0.008436344
0.02024	2.01434	2.016323614	0.098474625
0.02503	1.84731	1.843603922	0.200620278
0.03016	1.70964	1.702925891	0.392720604
0.03975	1.53117	1.535536765	0.285191390
0.05165	1.39020	1.383829617	0.458235034
0.05993	1.29365	1.306465376	0.990637025
0.08087	1.16284	1.170239721	0.636349021
0.10118	1.08208	1.093826204	1.085520823
0.15112	0.94127	0.931835667	1.002298304
0.20106	0.82628	0.825969185	0.037616138
0.25516	0.78375	0.784853861	0.140843515
0.29957	0.75021	0.750432515	0.029660304
0.40424	0.73599	0.735017964	0.132071938
0.49988	0.73264	0.731860959	0.106333412
0.59525	0.75021	0.750034016	0.02345799
0.79382	0.79889	0.798782400	0.013468651
1.00507	0.85851	0.852316439	0.721431431

2.2 Mesh Sensitivity Analysis

To ensure accurate finite element simulation results, a mesh sensitivity study was performed by progressively refining the mesh and analyzing its impact on stress distribution at the vertex region. Different mesh densities were assessed, and convergence was evaluated by tracking variations in stress with respect to normalized distance. The results showed that convergence was attained once the element count exceeded approximately 380,000 to 401,000, beyond which the stress values remained consistent, matching up to the second decimal point (Figure 5).

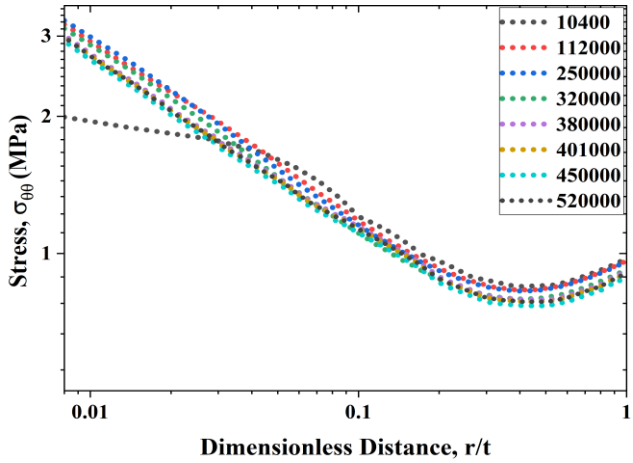

Figure 5: Evaluation of mesh sensitivity

In this study, finite element analysis (FEA) utilized C3D8E elements, which are 8-node linear brick elements with enhanced hourglass control. These elements were selected for their ability to accurately model stress distributions in complex geometries under various loads, with nodes allowing movement in the X, Y, and Z directions. Each model used around 412,800 elements, totaling 1,295,298 degrees of freedom, carefully balancing computational efficiency and accuracy. Consistent mesh configurations and element types were used across all scenarios, ensuring direct comparisons and uniform discretization accuracy. Attention to potential modeling and discretization errors in FEA was crucial for accurate simulation outcomes. Mesh Discretization Error, especially in regions near vertices with elevated stress, an

enhanced meshing approach was adopted. This included targeted mesh seeding, numerical biasing, sensitivity evaluations, and convergence analysis. Selecting appropriate element types was vital for maintaining result fidelity, especially in regions with steep gradients. To ensure analysis stability and minimize numerical errors, careful monitoring prevented non-convergence, divergence, or significant residual forces throughout the computational process. Continuous solver convergence checks and adherence to specified tolerance levels ensured equilibrium in all simulation increments.

3. RESULTS AND DISCUSSION

Differing in upper adherend composition Gallium Nitride and Indium Nitride with a common Silicon Carbide lower adherend, known for superior mechanical and thermal properties, these joints are meticulously analyzed for material selection. Emphasizing the suitability and unique attributes of Gallium Nitride and Indium Nitride, renowned in high-performance electronic devices, enhances overall joint performance. The research further investigates the impact of altering interlayer thickness on singular stress distribution. Systematic changes are explored through experiments, utilizing advanced computational approaches such as the FEM analysis and ABAQUS simulation software. Stress simulation at various locations reveals patterns on a graph, depicting stress distribution against angles (φ) and radial distances (r), offering insights into interlayer thickness-related trends.

The study delves into the analysis of tensor stresses $\sigma_{\theta\theta}$, $\sigma_{r\theta}$ & $\sigma_{\theta\varphi}$ in both upper and lower interfaces. Using Abaqus, a circular path was created with ϕ set at a radial distance r=1. The data analysis involved extracting the dataset for a detailed exploration of tensor stresses. Measured stress tensors across Gallium Nitride-resin, Indium Nitride-resin, and both resin-silicon Carbide interfaces, accounting for varying bonded thickness, facilitating comparisons across materials and structures.

3.1 Distribution of Stresses σij, Against Angle ϕ

The distribution of stresses for varying interlayer thicknesses within the varying thickness limit, ranging from 10 nm to 100 nm, is shown in Figure 6. In Figure 6, the 100 nm thickness across all interfaces exhibits the highest value, diminishing as thickness decreases. Comparatively, the maximum tensor stress value ($\sigma_{\theta\theta}$) at 100nm is approximately 3.66 MPa for the GaN-Resin interface, while the Resin-Sic interface on the GaN upper substrate registers at 3.38 MPa. Similarly, for the InN-Resin interface, $\sigma_{\theta\theta}$ peaks at around 2.55 MPa, whereas the Resin-Sic interface on the InN upper substrate records 2.07 MPa. Stress levels decline from 0˚ to 44˚ and rise from 46˚ to 90˚, following a consistent pattern. Stresses also gradually decrease for 40, 20, and 10 nm. Also, the 10nm thickness curves exhibit curvature, possibly indicative of the L-shape model.

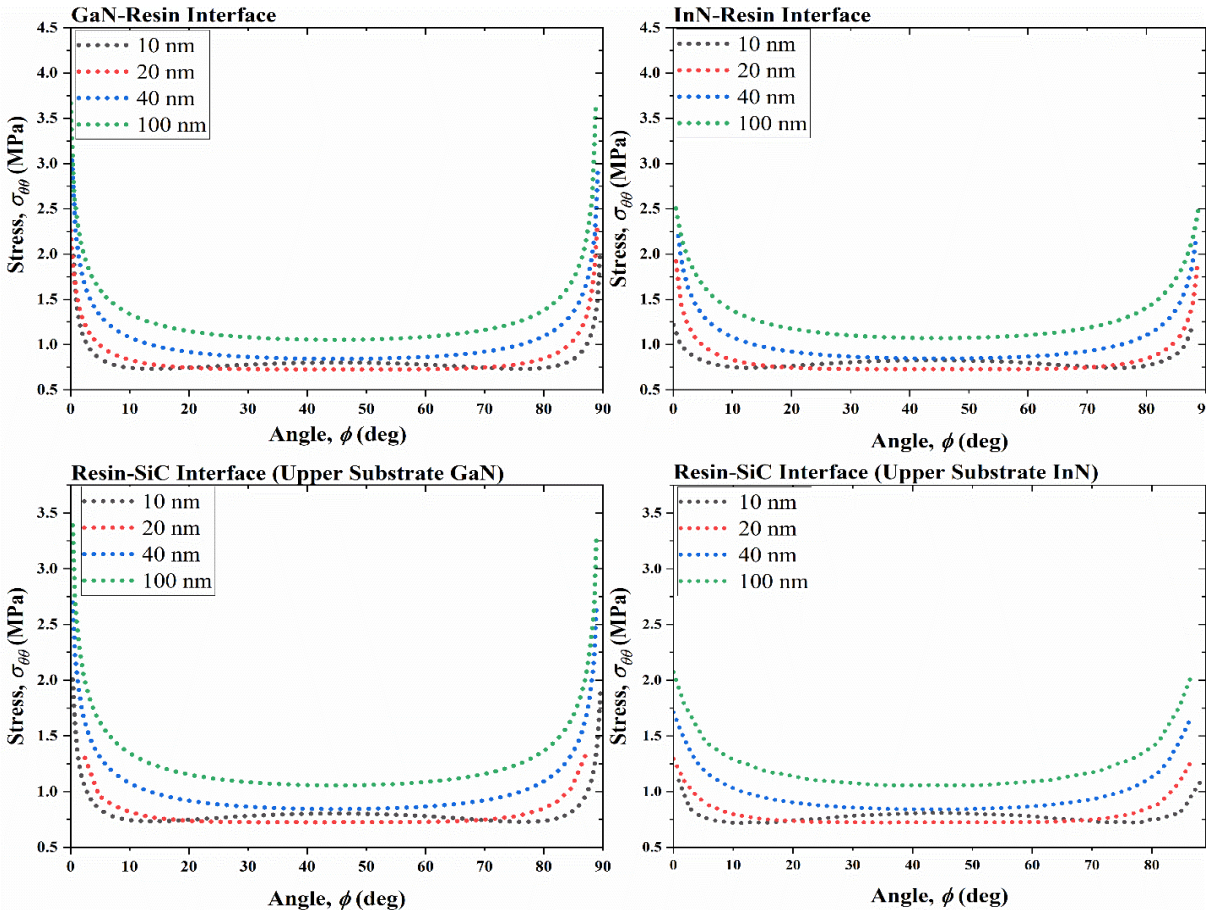

Figure 6. Distribution of Stress, $\sigma_{\theta\theta}$ against angle, ϕ-deg for varying interlayer thicknesses

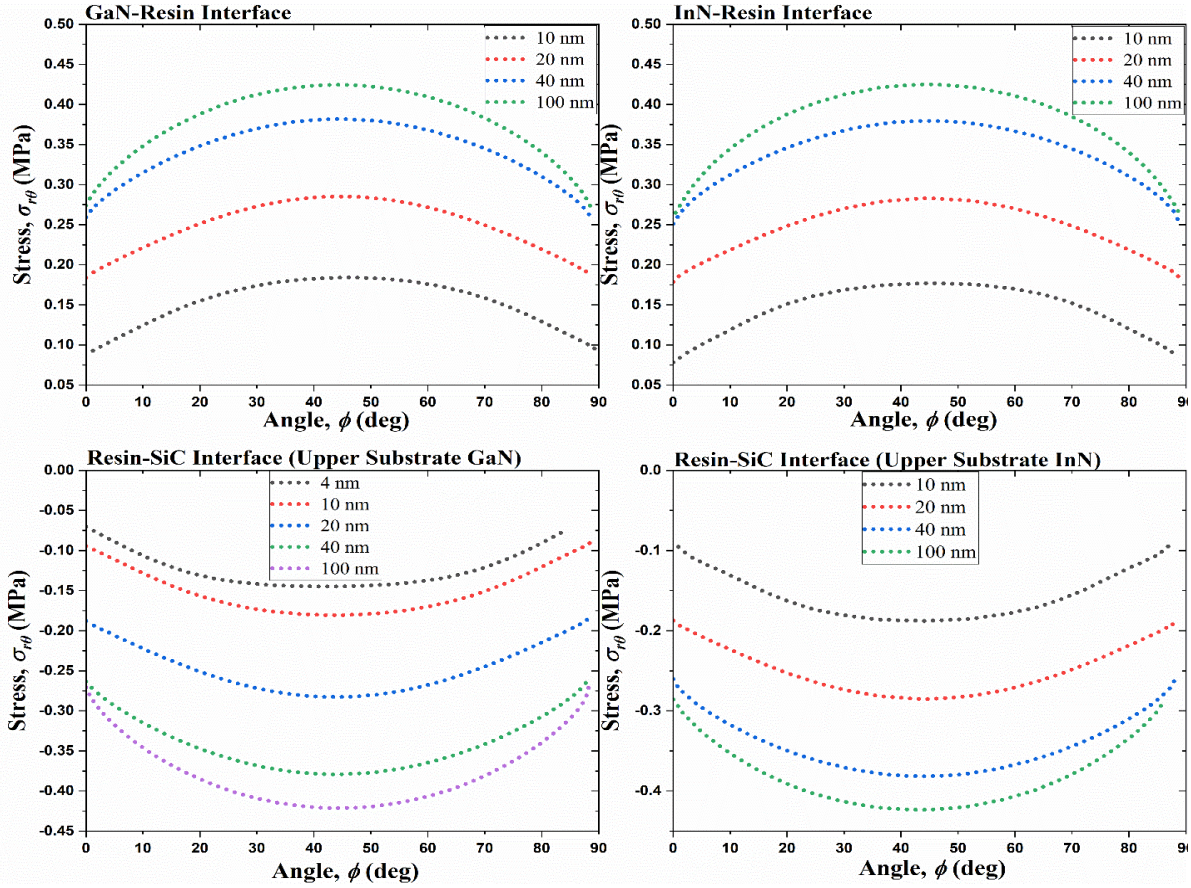

Figure 7. Distribution of Stress, $\sigma_{\theta\theta}$ against angle, ϕ-deg for varying interlayer thicknesses

The distribution of stress, $\sigma_{r\theta}$, against angle, ϕ for varying interlayer thicknesses with radial distance r=1nm is presented in Figure 7. The limit of analysis was within 10 nm up to 100 nm. This figure exhibits symmetric, parabolic profiles centered around ϕ=45°, indicating inflection points where shear stress peaks (tensile at the resin interfaces, compressive at Resin–SiC interfaces). Stress magnitude increases with thickness, highlighting greater interfacial stress transfer with thicker interlayers. GaN-based interfaces show higher stress levels than InN-based ones, suggesting stronger mechanical mismatch or stiffer behavior. No angular asymmetry is observed, implying isotropic material response and symmetric boundary conditions. Similarly, the distribution of stress, $\sigma_{\theta\varphi}$, against angleϕ for varying interlayer thicknesses with radial distance r=1nm within the thickness 1 to 100 mm is shown in Figure 8. It is noted that (Figure 8), stresses across interfaces and thicknesses peak at 0˚, sharply decreasing to near zero by 45˚ and further diminishing after 46˚ to 90˚. Generally, the highest stress patterns occur at 100nm (both at positive and negative ends), gradually decreasing for 40, 20, 10, 4, and 2nm. Comparative interface graphs are presented in Figure 8. The data can provide a comparison-based analysis for both variants (Gallium Nitride and Indium Nitride) as well as the optimum thickness choices for adhesive to be used. For instance, the stress distribution $\sigma_{\theta\theta}$, $\sigma_{r\theta}$, $\sigma_{\theta\varphi}$ at 100 nm has the highest value found compared to other thicknesses. The Distribution against a 90º angle can also provide an overview of vertex and interfacial edges.

Figure 9 shows the distribution of Stress, σij, against angle θ for varying interlayer thicknesses with radial distance r=1nm. The 180^0 angle stress distribution is essentially required to get a complete overview. In Figure 9(a), $\sigma_{\theta\theta}$ peaks sharply between 70°–90°, especially for thicker adhesive layers, indicating greater stress concentration near the interface vertex. An inflection near 100° marks a transition zone where stress begins to decline, and the curve's asymmetry reflects directional stress transfer inherent to the L-shaped joint geometry. Figure 9(b) shows $\sigma_{r\theta}$ transitioning from positive to negative near 100°, with a maximum around 60°, suggesting shear reversal. Figure 9(c) illustrates similar behavior in $\sigma_{\theta\varphi}$, with a primary peak near 60° and a secondary dip around 120°–140°, both diminishing with thinner adhesives. These localized features confirm that adhesive thickness strongly influences stress gradients and singularities across trimaterial interfaces, highlighting the need for precise thickness control to mitigate failure risks in nano-scale semiconductor joints.

Three-dimensional graphs were plotted in Figure 10 to analyze each tensor stress curve on interconnection surfaces. The $\sigma_{\theta\theta}$, $\sigma_{r\theta}$ & $\sigma_{\theta\varphi}$ of both connecting surfaces of Gallium Nitride is being demonstrated.

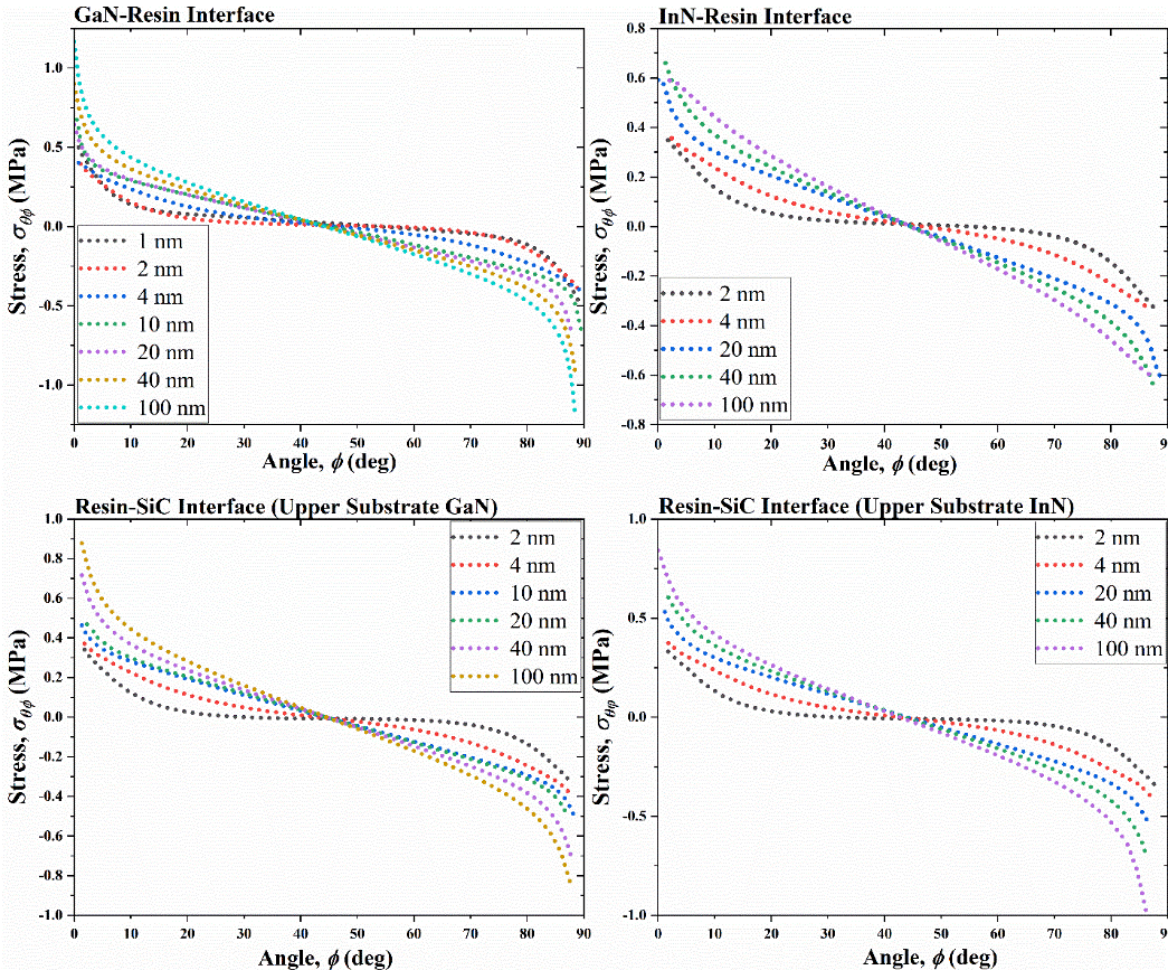

Figure 8. Distribution of Stress, $\sigma_{\theta\varphi}$, against angle, ϕ-deg for varying interlayer thicknesses

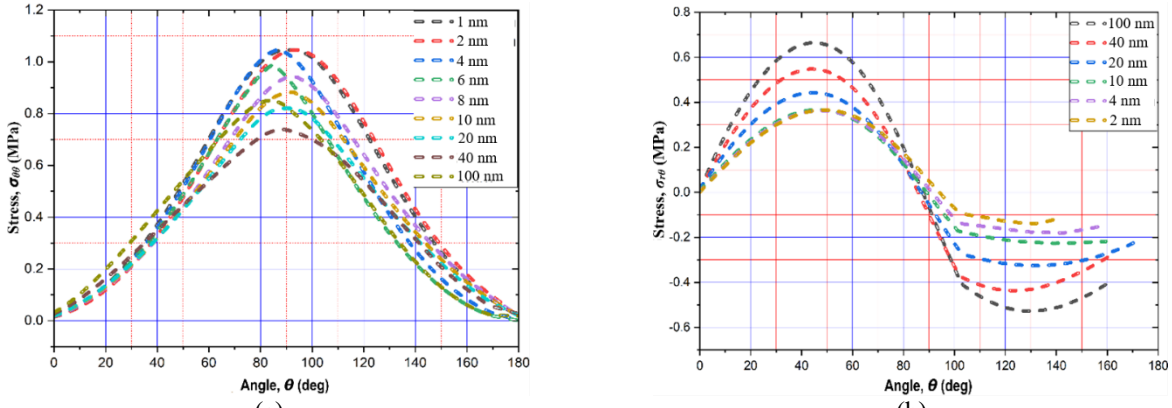

(a) (b)

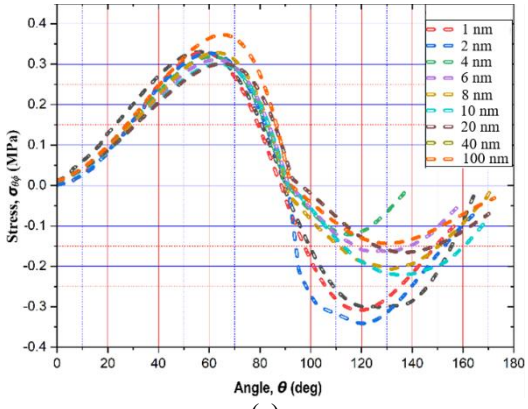

(c)

Figure 9. Distribution of stress, σij, against θ-deg (=180°) for (a) $\sigma_{\theta\theta}$ (b) $\sigma_{r\theta}$ and (c) $\sigma_{\theta\varphi}$

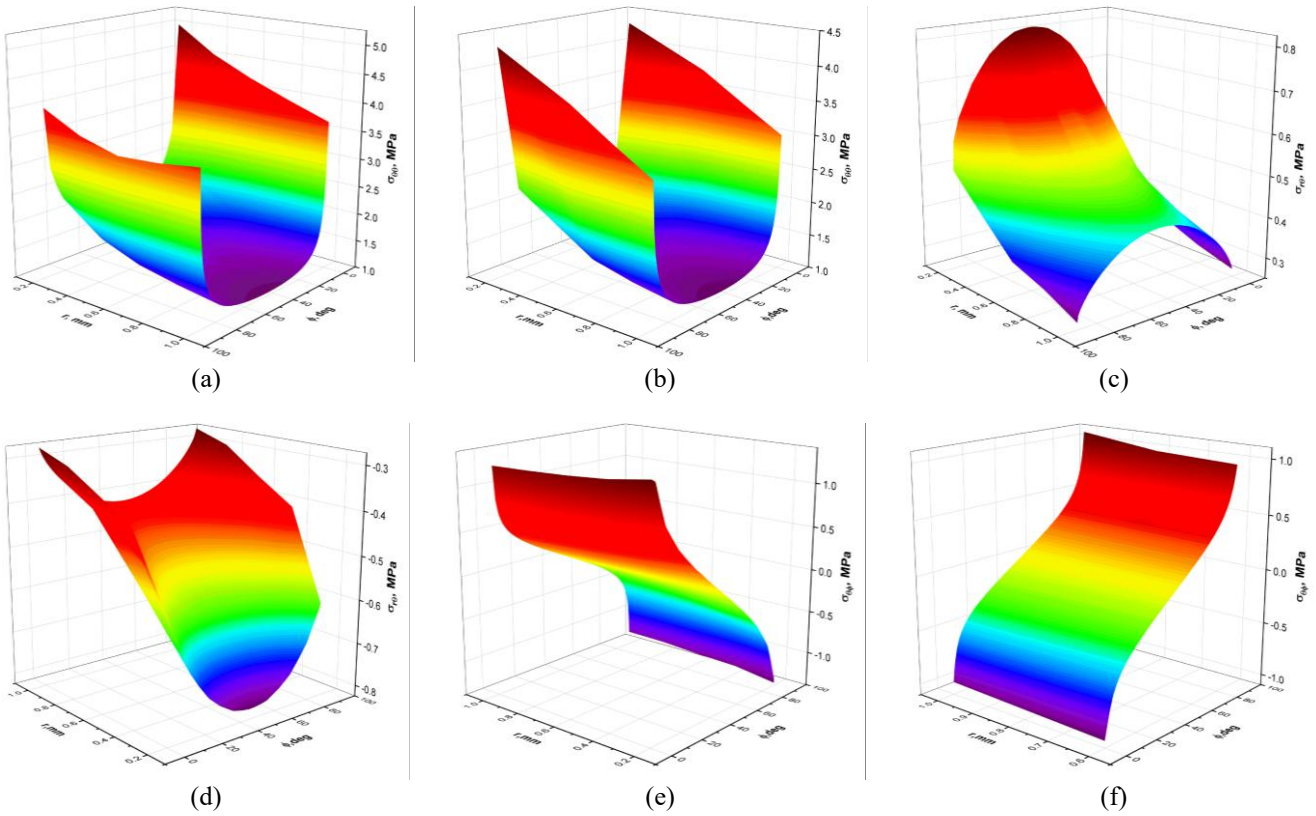

Figure 10. Dispersion of 3D stresses in accordance with interfaces. (a) $\sigma_{\theta\theta}$ at Gallium-Resin (b) $\sigma_{\theta\theta}$ at Resin-Silicon (c) $\sigma_{r\theta}$ at Gallium-Resin (d) $\sigma_{r\theta}$ at Resin-Silicon (e) $\sigma_{\theta\varphi}$ at Gallium-Resin (f) $\sigma_{\theta\varphi}$ at Resin-Silicon

3.2 Analysis of the Stress, σij, Against r/t for Different Interlayer Thickness

This research explores the evaluation of tensor-based stress components in both upper and lower interfaces. A circular trajectory was generated within Abaqus simulation software with ϕ set at 45º (for $\sigma_{\theta\theta}$, $\sigma_{r\theta}$) and 30º (for $\sigma_{\theta\varphi}$). The meticulous data analysis involved extracting and examining the dataset for a detailed exploration of tensor stresses across Gallium Nitride-resin, Indium Nitride-resin, and their resin-silicon Carbide interfaces, accounting for varying bonded thickness were being used for utilization of the dimensionless distance *r*/t. Figure 11 illustrates the variation of circumferential stress ($\sigma_{\theta\theta}$) with respect to the normalized distance (r/t) at an angle of ϕ =45º. The analysis was carried out for a thickness limit of 2 nm to 100 nm achieved using FEM are given.

Figure 11 illustrates Stress ($\sigma_{\theta\theta}$) plotted against dimensionless distance, ranging from 0.01 to 1.1 for GaN-Resin and InN-Resin interfaces and from 0.02 to 1.1 for their Resin-SiC interfaces. The stress patterns, plotted across adhesive thicknesses from 2nm to 100nm, show a maximum of 100nm, gradually decreasing with reduced thickness. The peak stress value for the GaN-Resin interface initiates at 2.43 at 0.01, while the InN-Resin interface starts at 2.27. The stress values for Resin-SiC interfaces on upper substrates GaN and InN are 1.9 and 1.87, respectively.

Figure 12 shows the distribution of Stress, $\sigma_{r\theta}$, against dimensionless distance, *r*/t for angle ϕ=45º. This analysis was within the thickness limit, ranging from 2 nm to 100 nm. The graphical representation of stress distribution ($\sigma_{r\theta}$) spans a dimensionless distance from 0.01 to 1, encompassing adhesive thicknesses from 2nm to 100nm. Notably, stress levels decrease proportionally with diminishing thickness. The stress curvatures exhibited a decreasing trend. The stress patterns at GaN-Resin and InN-Resin interfaces show close similarities, appearing relatively stable. However, minor deviations in stress trends occur for Resin-SiC interfaces with changes in thicknesses.

The distribution of stress, $\sigma_{\theta\phi}$, against dimensionless distance, *r*/t for angle ϕ=30º is shown in Figure 13. The plots are shown within the limit of thickness ranging from 2nm to 100nm achieved. Figure 13 displays graphs ranging from 2nm to 100nm for interfaces with GaN as the upper adherend. It reveals critical localized features: the stress is highest for the 100 nm thickness (like others), decreasing with thinner layers, reflecting greater stress concentration in thicker adhesives due to increased resin volume; inflection points indicate a transition from a steep stress drop near the vertex to a gradual decline, likely tied to the L-shaped model's geometry enhancing stress singularity, with thinner layers showing reduced inflection intensity, suggesting mitigated stress gradients; subtle asymmetries in thicker layers likely from GaN's stiffer properties versus resin, indicating uneven stress distribution and potential failure risk, which diminishes in thinner layers, implying improved uniformity; and a sharp peak near r/t = 0.01 for 100 nm highlights vertex stress concentration, relaxing to near zero with distance, underscoring the need for thickness optimization to enhance nano-scale joint reliability.

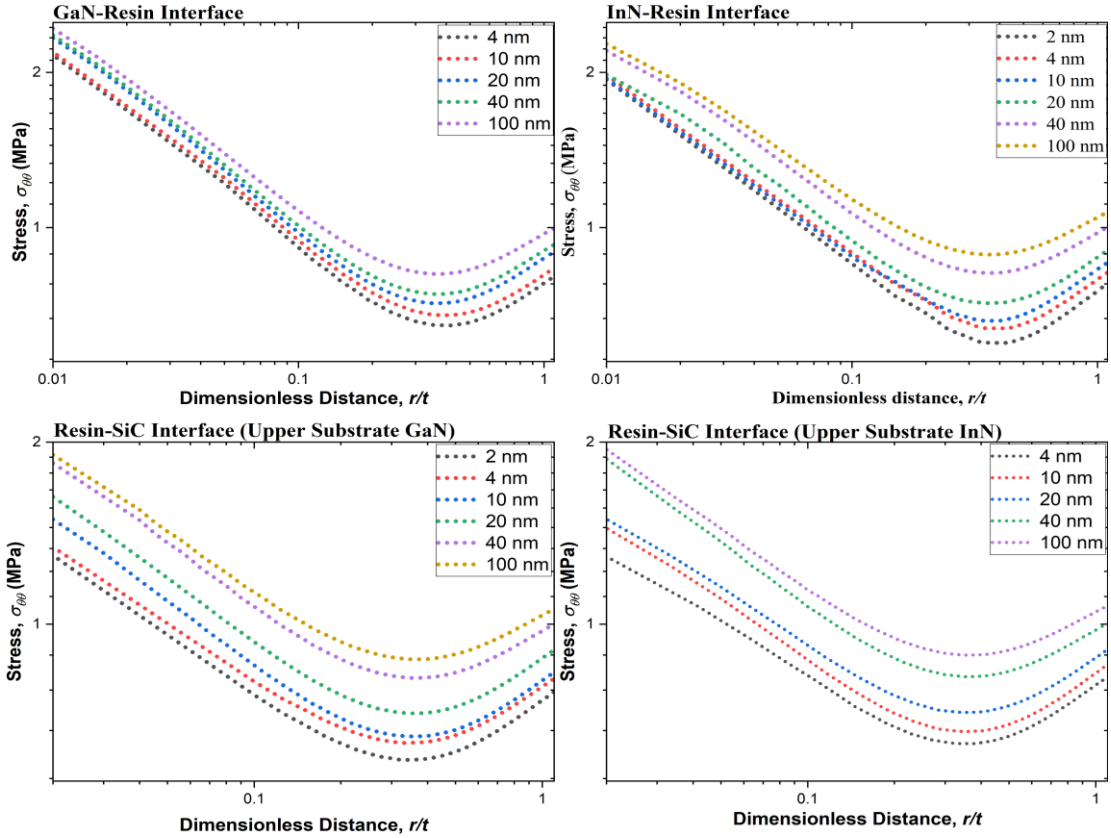

Figure 11. Distribution of Stress, $\sigma_{\theta\theta}$, against dimensionless distance r/t of interfaces regarding varying interlayer thicknesses

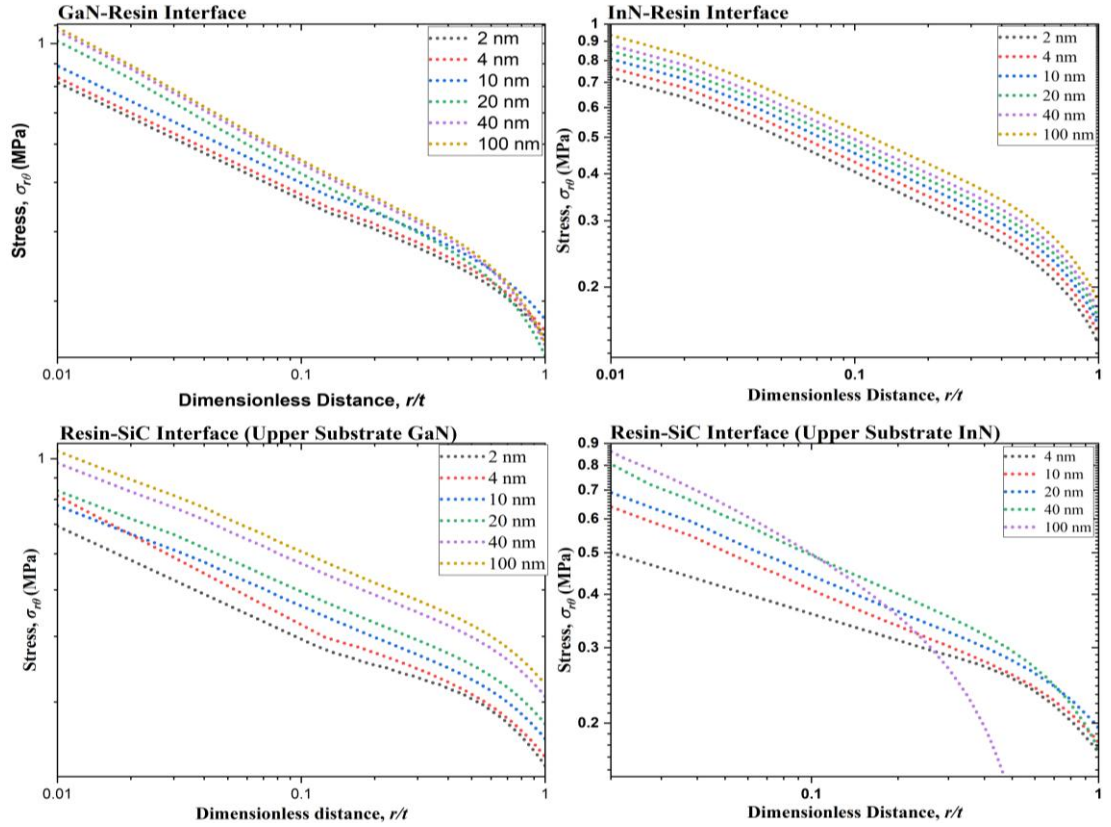

Figure 12. Distribution of Stress, $\sigma_{r\theta}$, against dimensionless distance r/t of interfaces regarding varying interlayer

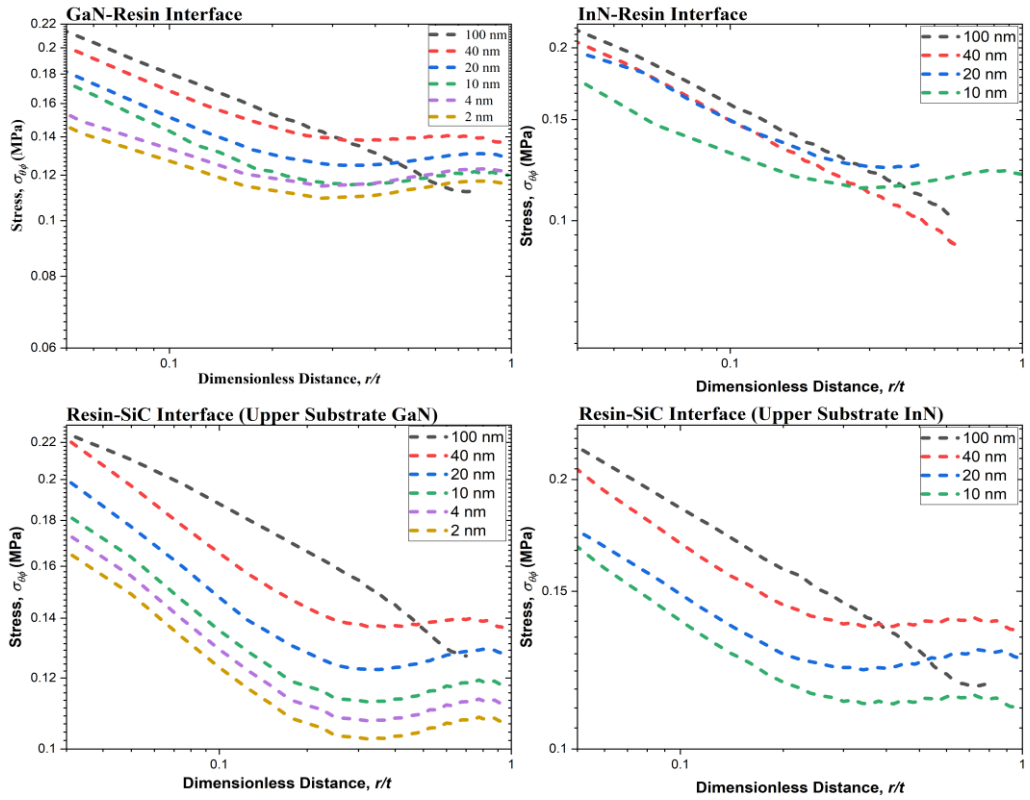

Figure 13. Distribution of Stress, $\sigma_{\theta\phi}$, against dimensionless distance r/t of interfaces regarding varying interlayer

In contrast, the graphs corresponding to interface configurations featuring InN as the upper adherend are shown for thicknesses ranging from 10 nm to 100 nm. For Figure 11, the singular stress region in the Gallium Nitride–Resin interface is confined to r/t < 0.45, while for the Silicon–Resin interface, it remains limited to r/t < 0.35. The same distribution changes happened in the case of the Indium Nitride substance. The stress magnitude reached approximately. 1 MPa, as well as the inflection points of $\sigma_{\theta\phi}$ singularity are similar to those of Stress $\sigma_{\theta\theta}$. Also, there nothing has been found for $\sigma_{r\theta}$ distribution. The $\sigma_{r\theta}$ & $\sigma_{\theta\phi}$ are both visualized in Figures 12 and 13. $\sigma_{\theta\theta}$ & $\sigma_{r\theta}$, distribution angles were taken at 45° whereas for $\sigma_{\theta\phi}$ that was being taken at 30° because the value of 45° happened to be 0.

3.3 Analysis of Intensity of Singularity, k, for Varying Interlayer Thicknesses

A correlation involving the singularity intensity in the radial direction, *Kij*, for each interfacial edge against diversified thicknesses ranging up to 10 mm is shown in Figure 14. It is found that $k_{\theta\theta}$ is larger than $k_{r\theta}$ and $k_{\varphi\theta}$. The intensity varies upon the thickness, t in both cases: Gallium Nitride and Indium Nitride. As the interlayer thickness decreases, singularity intensity diminishes, suggesting a reciprocal reduction through interaction. Examining interface distributions reveals a more pronounced decrease in the gallium nitride-resin interface compared to the resin-silicon interface. This highlights a notable interaction effect, particularly when Gallium Nitride-Resin and Resin-Silicon interfaces approach each other. Similarly, the case applied to the interface between Indium Nitride-Resin and the Resin-Silicon amalgamation.

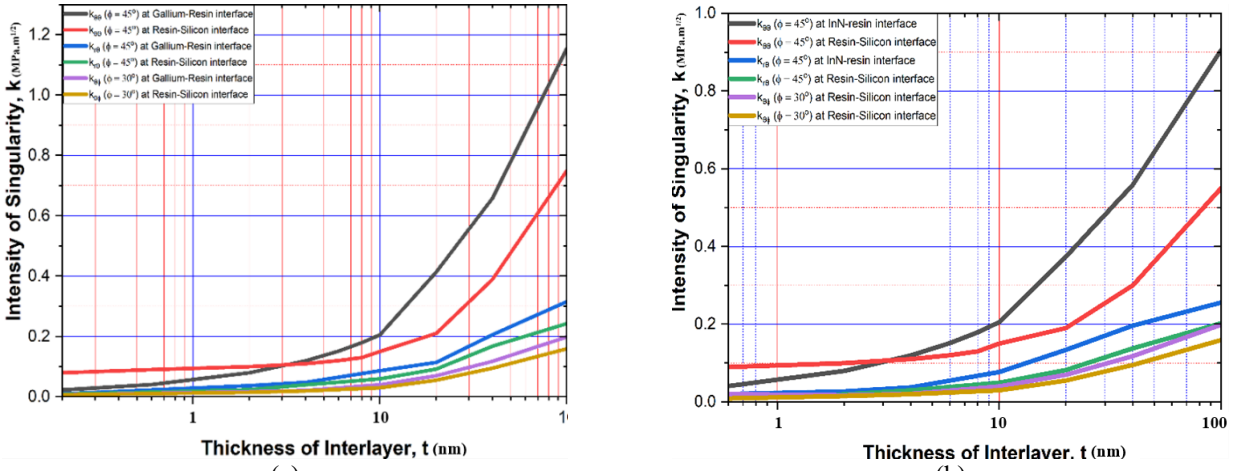

(a) (b)

Figure 14. Correlation of singularity intensity at interfacial edges with varying thicknesses where higher adherend is (a) Gallium Nitride, (b) Indium Nitride

4. CONCLUSIONS

This study analyzed the stress distribution of a three-layer adhesively bonded joint—the distribution along the radial distance and angle. The impact of altering the thickness of the intermediary and variations in the upper adherend's properties provide a comprehensive analysis. The singularity of the stress field was investigated. The outcome of this analysis is summarized below:

- The highest magnitudes of stress and deformation have been found in the proximity of the interface's vertex and along its edges. The stress distribution changes with different interlayer thicknesses. An increase in adhesive layer thickness resulted in higher observed stress levels.
- The GaN model showed higher stress levels for the same adhesive thickness than the InN model at the vertex. However, the stress trends were found to be quite similar for both models.
- As the interlayer thickness decreases, singularity intensity drops due to interaction effects, with a more significant reduction observed at the Gallium Nitride-Resin interface compared to the Resin-Silicon interface and similarly for the Indium Nitride-Resin interface.

ACKNOWLEDGEMENTS

The authors express their gratitude to the Department of Mechanical Engineering at Khulna University of Engineering & Technology for offering computational resources and technical support.

CONFLICT OF INTEREST

The authors declare that they have no financial or non-financial conflicts of interest related to this work.

AUTHORS CONTRIBUTION

Shah Mohammad Azam Rishad : Investigation, data acquisition, analysis, writing- original draft, editing.

Md Shahidul Islam: Review and editing, writing, supervising.

Md. Ashraful Islam: Writing, reviewing and editing, Supervising.

REFERENCES

[1] M.D. Banea and L.F.M. Da Silva, "Adhesively bonded joints in composite materials: an overview," *Proceedings of the Institution of Mechanical Engineers, Part L: Journal of Materials: Design and Applications*, vol. 223, no. 1, pp. 1-18, 2009.

[2] W. Guo, P. Chen, L. Yu, G. Peng, Y. Zhao, and F. Gao, "Numerical analysis of the strength and interfacial behaviour of adhesively bonded joints with varying bondline thicknesses," *International Journal of Adhesion and Adhesives*, vol. 98, p. 102553, 2020.

[3] L.F.M. Da Silva, A. Öchsner, and R.D. Adams, "Introduction to adhesive bonding technology," in *Handbook of Adhesion Technology*, L. F. M. da Silva, A. Öchsner, R. D. Adams, Berlin, Heidelberg: Springer, 2011, pp. 1-7.

[4] L. Guo, J. Liu, H. Xia, X. Li, X. Zhang, and H. Yang, "Effects of surface treatment and adhesive thickness on the shear strength of precision bonded joints," *Polymer Testing*, vol. 94, p. 107063, 2021.

[5] D.B. Lee, T. Ikeda, N. Miyazaki, and N. Choi, "Effect of Bond Thickness on the Fracture Toughness of Adhesive Joints," *Journal of Engineering Materials and Technology*, vol. 126, no. 1, pp. 14-18, 2004.

[6] L. Liao, C. Huang, and T. Sawa, "Effect of adhesive thickness, adhesive type and scarf angle on the mechanical properties of scarf adhesive joints," *International Journal of Solids and Structures*, vol. 50, no. 25, pp. 4333-4340, 2013.

[7] X. Shen, Z. Xia, and F. Ellyin, "Cyclic deformation behavior of an Epoxy polymer. Part I: Experimental investigation," *Polymer Engineering & Science*, vol. 44, pp. 2240-2246, 2004.

[8] B. Chen, Q. Yuan, and J. Luo, "Stress concentration in adhesive layer of adhesively bonded piezoelectric pipe-joint system," *Journal of Superconductivity and Novel Magnetism*, vol. 23, no. 6, pp. 945-947, 2010.

[9] C. Lin and K. M. Liechti, "Similarity concepts in the fatigue fracture of adhesively bonded joints," *The Journal of Adhesion*, vol. 21, no. 1, pp. 1-24, 1987.

[10] H. Koguchi and K. Yokoyama, "Stress analysis in three-dimensional joints with a crack at the vertex of the interface," *Acta Mechanica*, vol. 228, no. 8, pp. 2759-2773, 2017.

[11] M. Uddin, M. Ali, and H. P. Chan, "Achieving optimum adhesion of conductive adhesive bonded flip-chip on flex packages," *Reviews on Advanced Materials Science*, vol. 21, pp. 165-172, 2009.

[12] H. Koguchi and J. A. da Costa, "Analysis of the stress singularity field at a vertex in 3D-bonded structures having a slanted side surface," *International Journal of Solids and Structures*, vol. 47, no. 22, pp. 3131-3140, 2010.

[13] M. S. Islam and H. Koguchi, "Analysis of intensity of singularity at a vertex in 3d transversely isotropic piezoelectric bimaterial joints by boundary element method," in *2013 International Conference on Informatics, Electronics and Vision (ICIEV)*, Dhaka, Bangladesh, 2013.

[14] M. S. Islam, M. G. Kader, M. M. K. Uddin, and M. Ahmed, "Analysis of order of stress singularity at a vertex in 3d transversely isotropic piezoelectric dissimilar bonded joints," *Journal of Mechanical Engineering*, vol. 44, no. 1, pp. 1-5, 2014.

[15] X. Lan and N. A. Noda, "Effects of resin thickness on the stress intensity factors of edge-cracked adhesive joints," in *2014 15th International Conference on Electronic Packaging Technology*, Chengdu, China, 2014.

[16] Y. Zhang, P. Wu, and M. Duan, "A mesh-independent technique to evaluate stress singularities in adhesive joints," *International Journal of Adhesion and Adhesives*, vol. 57, pp. 105-117, 2015.

[17] S. Kundurthi and M. Haq, "Substrate thickness optimization in multi-material single lap adhesive joints," *Journal of Applied Mechanics*, vol. 91, no. 5, p. 051007, 2024.

[18] J. Korbel, R. Kochetov, and X. Dong, "Aluminum-epoxy bonding strength assessment based on modified butt joint sample," in *2024 IEEE Electrical Insulation Conference (EIC)*, Minneapolis, MN, USA, pp 264-268, 2024.

[19] S. Toshiyuki, I. Higuchi, and J. Shimura, "Three-dimensional finite element analysis of stress response in adhesive scarf joints subjected to impact tensile loads," in *Adhesive Joints: Formation, Characteristics and Testing 2023*, K. L. Mittal, London: CRC Press, pp. 257-272, 2002.

[20] N. Noda, R. Takaki, Y. Sano, and B. Wang, "ISSF method to evaluate adhesive strength when two distinct singular stress fields appear along the interface," *International Journal of Fracture*, vol. 241, pp. 95–114, 2023.

[21] K. Demir, E. Gavgali, A. F. Yetim, and S. Akpinar, "The effects of nano-structure additive on fracture strength in adhesively bonded joints subjected to fully reversed four-point bending fatigue load," *International Journal of Adhesion and Adhesives*, vol. 110, p. 102943, 2021.

[22] M. Martinez, "Finite element model of structures with piezoelectric elements," Ph.D. Thesis, Carleton University, Canada, 2006.

[23] G. C. Lyu, B. Chen, X. Zhang, M. Zhou, C. Ke, and Y. Mai, "An extensive study of the effects of packaging structure and material properties on reliability of advanced packages by charactering the stress singularities at interface corners," in *2023 IEEE 25th Electronics Packaging Technology Conference (EPTC)*, Singapore, 2023.

[24] S. M. A. Rishad, M. S. Islam, and M. A. Islam, "Evaluation of stress distributions in trimaterial bonded joints with nano-resin adhesive using machine learning models," *Results in Materials*, vol. 23, p. 100618, 2024.

[25] S. M. A. Rishad, M. A. Islam, and M. S. Islam, "Analysis of stress distribution of CFRP bonded joints: a study of numerical and machine learning approach," *Heliyon*, vol. 11, no. 3, p. e42440, 2025.

[26] J. Valdoleiros, A. A. Safar, P. Maleki, P. F. C. Videira, R. J. C. Carbas, E. A. S. Marques, et al., "Effects of temperature on the fracture response of EMC-Si interface found in multilayer semiconductor components," *Surfaces*, vol. 8, no. 1, p. 2, 2025.

[27] G. C. Lyu, X. P. Zhang, M. B. Zhou, C. B. Ke, and Y. W. Mai, "Prediction of crack initiation at die corner of molded underfill flip-chip packages under thermal load by new criteria," *IEEE Transactions on Device and Materials Reliability*, vol. 24, no. 4, pp. 498-506, 2024.

[28] H. Koguchi and M. Nakajima, "Influence of interlayer thickness on the intensity of singular stress field in 3d three-layered joints under an external load," *Journal of Solid Mechanics and Materials Engineering*, vol. 4, no.7, pp. 1027-1039, 2010.

[29] I. Yonenaga, Y. Ohkubo, M. Deura, K. Kutsukake, Y. Tokumoto, Y. Ohno, et al., "Elastic properties of indium nitrides grown on sapphire substrates determined by nano-indentation: In comparison with other nitrides," *AIP Advances*, vol. 5, p. 077131, 2015.

[30] I. Bhat, "3 - Physical properties of gallium nitride and related III–V nitrides," in *Wide Bandgap Semiconductor Power Devices*, B.J. Baliga, Woodhead Publishing, 2019, pp. 43-77.

[31] [cited 2024 January 6]; Available from: https://en.wikipedia.org/wiki/Indium_nitride.

[32] S. Bhatia, S. Angra, and S. Khan, "Mechanical and wear properties of epoxy matrix composite reinforced with varying ratios of solid glass microspheres," *Journal of Physics: Conference Series*, vol. 1240, 2019.

[33] [cited 2024 March 6]; Available from: https://pubchem.ncbi.nlm.nih.gov/compound/Silicon-carbide.